Journal of Applied Polymer Science

Investigation of the Crystallization Behavior of Isotactic Polypropylene Polymerized with Different Ziegler-Natta Catalysts

Jian Kang, Jingping Li, Shaohua Chen, Hongmei Peng, Bin Wang, Ya Cao, Huilin Li, Jinyao Chen, Jinggang Gai, Feng Yang, Ming Xiang

State Key Laboratory of Polymer Materials Engineering, Polymer Research Institute of Sichuan University, Chengdu 610065, People's Republic of China

Correspondence to: Dr. F. Yang (E-mail: yangfengscu@126.com) or M. Xiang (E-mail: xiangming45@hotmail.com)

ABSTRACT: Detailed characterization of the crystallization behavior is important for obtaining better structure property correlations of the isotactic polypropylene (iPP), however, attributed to the complexity in ZN-iPP polymerization, the relationship between crystallization behavior and the stereo-defect distribution of iPP is still under debate. In this study, the crystallization kinetics of the primary nucleation, crystal growth and overall crystallization of two iPP samples (PP-A and PP-B) with nearly same average isotacticity but different stereo-defect distribution (the stereo-defect distribution of PP-B is more uniform than PP-A) were investigated. The results of isothermal crystallization kinetics showed that the overall crystallization rate of PP-A was much higher than that of PP-B; but the analysis of self-nucleation isothermal crystallization kinetics and the polarized optical microscopy (POM) observation indicated that the high overall crystallization rate of PP-A was attributed to the high primary nucleation rate of the resin. The stereo-defect distribution plays an important role in determining both the nucleation kinetics and crystal grow kinetics, and thus influence the overall crystallization kinetics. A more uniform distribution of stereo-defects restrains the crystallization rate of iPP, moreover, it has more influence on nucleation kinetics, comparing with the crystal growth. © 2013 Wiley Periodicals, Inc. J. Appl. Polym. Sci. 129: 2663–2670, 2013

KEYWORDS: crystallization; morphology; polyolefins

Received 25 September 2012; accepted 2 January 2013; published online 30 January 2013
DOI: 10.1002/app.38984

INTRODUCTION

Isotactic polypropylene (iPP) is one of the most widely used polymers since Natta et al.[1] discovered the catalytic process necessary for the reaction of polymerization. Depending on the molecular structure,[2–4] thermal history,[5–7] and use of different nucleating agents,[8,9] iPP exhibits very interesting crystallization behavior and rather versatile polymorphic behavior, making it a material of choice for many commodity and specialty applications.

An important factor determining the crystallization behavior of iPP is the chain tacticity, including the average isotacticity and the defect distribution.[10,11] Therefore, the studies on the relationship between the molecular tacticity and the crystallization behavior of iPP are of great importance. In the past decades, great efforts had been made in this area. Since the catalytic mechanisms of the Ziegler-Natta (ZN) catalysts and Metallocene (MAO) catalysts were quite different, and the molecular structures of the obtained iPP were thus different,[12–14] the investigations were thus mainly performed around these two catalyst systems.

For ZN-iPP, great attention had been paid on the relationship between the average isotacticities and the crystallization behavior. Some researchers believed that the isotacticity has an important influence on the spherulitic morphology of iPP,[15] it also strongly affects the crystallization characteristics,[16,17] for instance, the number of crystal nuclei at the initial stage, crystallization dynamics, the morphology, size, and perfection of crystals in the final product, and can even induce variations in the nucleation mechanism and the fold surface free energy and the work of chain folding of iPP.[10,18] However, some other researchers held different point of view.[19,20] They thought that the overall crystallization rate is a direct function of the primary nucleation density, and would be correlated with nucleation density rather than microstructure of the iPP molecules.

Attributed to the complexity in ZN-iPP polymerization, it is not easy to only adjust the polymerization conditions and to obtain ZN-iPP samples with same average isotacticities, but different defect distributions. Therefore, the influence of stereo-defect distribution of ZN-iPP on the crystallization behavior

Table I. Molecular Structural Parameters of PP-A and PP-B

Sample	Catalyst	XS (%)[a]	Isotacticity ([mmmm]%)[b]
PP-A	ZN-A	3.8	96.6
PP-B	ZN-B	3.9	96.4

[a]Xylene soluble fraction at room temperature according to ASTM D5492;
[b]Isotacticity were obtained from high temperature ^{13}C-NMR at 120°C.

and crystallization kinetics are still under debate as far as we concerned, which is of great theoretical and practical importance.

In our previous study,[21] two iPP samples (PP-A and PP-B) were produced in Ziegler-Natta polymerization with different highly activity supported fourth generation Ziegler-Natta catalysts. The microstructures of the samples were characterized in detail and it was found that the average isotacticities of PP-A and PP-B were similar, but the stereo-defects distribution of PP-B was more uniform. Since the average isotacticities of PP-A and PP-B are similar, it is possible for us to study the influence of stereo-defect distribution on the crystallization behavior of the ZN-iPP clearly. In this study, the relationship between stereo-defect distribution and the crystallization behavior of ZN-iPP polymerized with different ZN catalysts are studied in detail.

EXPERIMENTAL

Materials

The preparation and microstructure characterization of the iPP samples used in this study was reported in the previous work.[21] The results of ^{13}C-NMR, successive self-nucleation and annealing, and FTIR had been discussed there in detail. A brief summary of the information of the samples is given here.

The iPP samples studied (PP-A and PP-B) were iPP for biaxially oriented polypropylene (BOPP) film. The average isotacticity information of PP-A and PP-B were listed in Table I. The tacticity information obtained from high resolution high temperature (HRHT) ^{13}C-NMR were shown in Table II. It can be observed from Tables I and II that, the average isotacticities of the samples are nearly same, but the stereo-defect distribution of PP-B is more uniform than PP-A. It was also found that, in the aspect of conformational behavior, the conformational order degree of PP-B is lower than that of PP-A.[21]

Characterization

Differential Scanning Calorimetry (DSC). All the calorimetric experiments were performed on Mettler Toledo DSC1 differential scanning calorimeter (DSC) under nitrogen atmosphere (50 mL/min). Temperature scale calibration was performed using indium as a standard to ensure reliability of the data obtained. The virgin polymer was molded at 190°C, 10 MPa for 5 min into sheets of uniform thickness about 500 μm, in order to ensure the homogeneity of the samples and the good contact between sample and pan. Then 5 mg round samples were punched out of the sheets.

Isothermal Crystallization Kinetics. The isothermal crystallization kinetics was performed according to the following procedures: (a) samples were heated to 200°C under a nitrogen atmosphere and kept for 5 min to erase any previous thermal history. (b) fast cooling down to a desired crystallization temperature at 50°C/min. (c) samples were isothermally kept for a period of time necessary to complete the crystallization.

Self-Nucleation Isothermal Crystallization Kinetics. The self-nucleation isothermal crystallization kinetics was performed following the procedures below.

First, the self-nucleating behavior of the samples was measured according to Fillon et al.,[22–24] and the temperature region for the self-nucleation domain (Domain II) was determined. Then, samples were held at 200°C for 5 min under a nitrogen atmosphere to destroy any residual nuclei. After that, samples were cooled to 30°C at 10°C/min and held for 2 min, to create "standard" thermal history, and heated again to the self-nucleating temperature (denoted as T_{SN}, the lowest temperature within Domain II is desired) and kept for 5 min. Then, it was rapidly cooled to a predetermined crystallization temperature (T_{cSN}) at 80°C/min and held for a period of time long enough to complete isothermal crystallization. Finally, the sample was heated to 200°C at a rate of 10°C/min. The thermal treatment protocol was shown in Scheme 1.

Polarized Optical Microscopy (POM). The superstructural morphology of the samples was studied with a ZEISS MC-80 polarized light microscope equipped with a LINKAMTP-91 hot-stage and a camera system. Thin melt-samples were prepared between microscope coverslips. They were melted at 200°C for 5 min and fast cooled (80°C/min) to isothermal crystallization temperature (denoted as T_c). To enhance contrast, a λ wave plate was inserted between the polarizers.

Table II. Tacticity Results of PP-B and PP-A Obtained from HRHT ^{13}C-NMR Measurement

	mm			mr			rr		
Sample[a]	mmmm	mmmr	rmmr	mmrr	mmrm+rmrr	rmrm	rrrr	mrrr	mrrm
PP-A	95.07	1.59	0.41	2.12	0.57	0.30	0.61	0.45	0.88
PP-B	94.78	1.47	0.53	2.17	0.71	0.31	0.65	0.48	0.90

[a]Samples were extracted in *n*–heptane for 24 h at desired temperature and then the insoluble fraction was collected and dried for HRHT ^{13}C-NMR measurement.

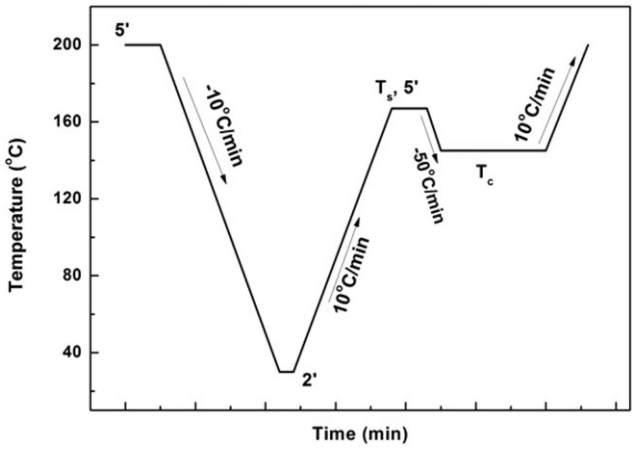

Scheme 1. Thermal treatment protocol of self-nucleation isothermal crystallization kinetics.

RESULTS AND DISCUSSION

Isothermal Crystallization Kinetics

The overall crystallization behavior of PP-A and PP-B were studied by means of isothermal crystallization kinetics. To ensure the feasibility, the isothermal crystallization temperature T_c should be well-chosen. For PP-A, the T_c interval was between 128 and 132°C; for PP-B, this interval shifts to lower crystallization temperatures, 123–127°C. The curves of the relative degree of crystallinity (X_t) as a function of crystallization time, and the corresponding exothermic DSC curves at these temperatures are presented in Figure 1. The X_t here is a relative value and could be defined as follows.

$$X_t = \int_0^t (dH/dt)\, dt \Big/ \int_0^\infty (dH/dt) dt \qquad (1)$$

Where dH_c denotes the measured enthalpy of crystallization during the isothermal time interval dt. The limits t and ∞ denotes the elapsed time during the course of crystallization and at the end of the crystallization process, respectively.

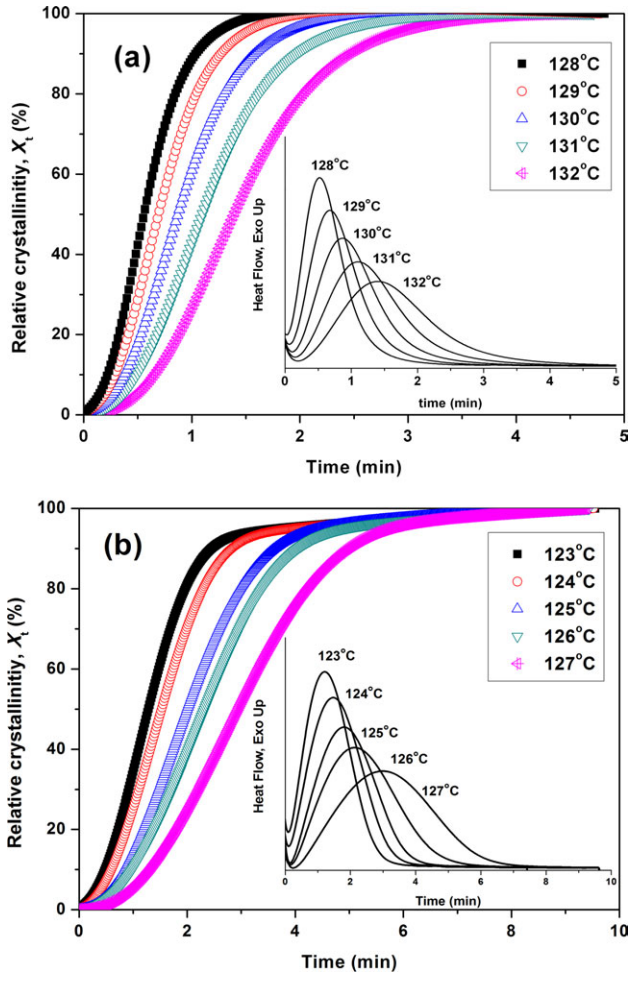

Figure 1. Plots of relative crystallinity versus crystallization time for (a) PP-A and (b) PP-B when isothermally crystallized at proper crystallization temperatures. Inset gives the corresponding exothermic DSC curves at these temperatures. [Color figure can be viewed in the online issue, which is available at wileyonlinelibrary.com.]

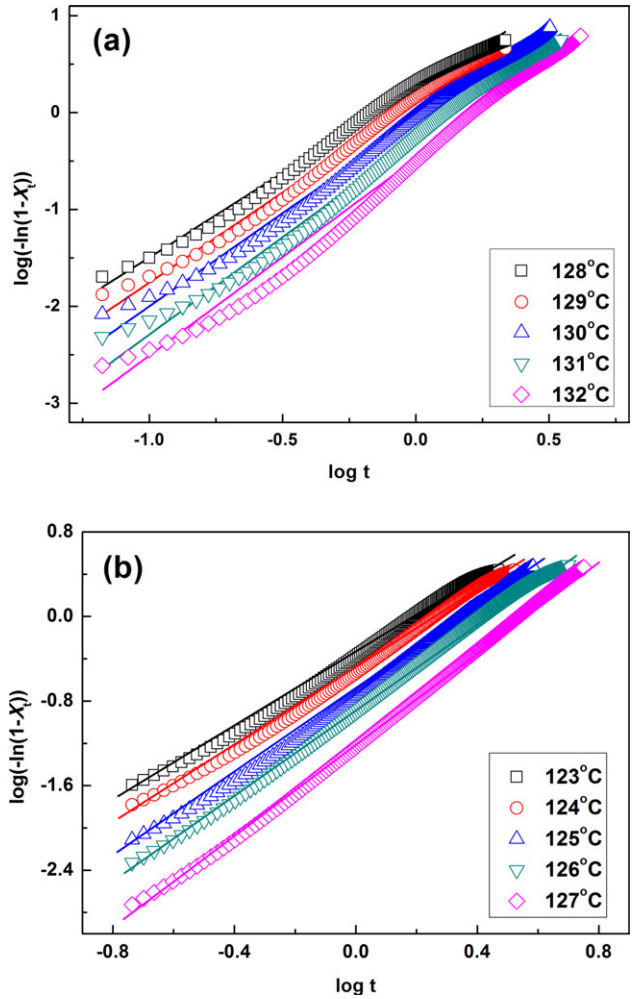

Figure 2. Avrami plots of log[-In(1-X_t)] versus log t for isothermal crystallization process for the samples (a) PP-A and (b) PP-B. [Color figure can be viewed in the online issue, which is available at wileyonlinelibrary.com.]

Applied Polymer SCIENCE

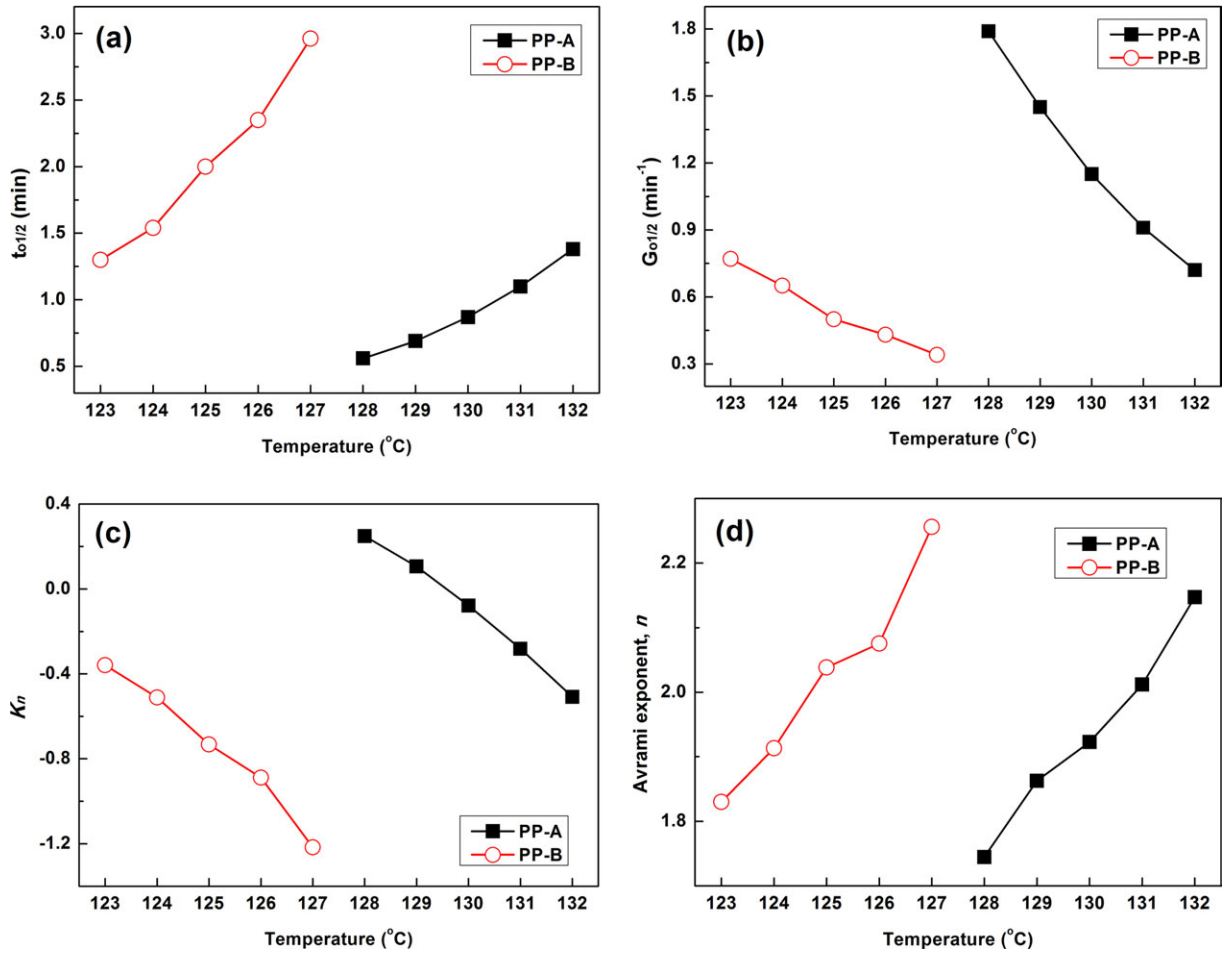

Figure 3. (a) The half-time of overall crystallization $t_{o1/2}$, (b) overall crystallization rate parameter $G_{o1/2}$, (c) crystallization rate parameter K_n and (d) Avrami exponent n as a function of isothermal crystallization temperature. [Color figure can be viewed in the online issue, which is available at wileyonlinelibrary.com.]

The half crystallization time ($t_{o1/2}$) of overall crystallization, which is defined as the half period (i.e., 50% crystallization), from the onset of crystallization and the end of crystallization, can be a direct measure of crystallization rate. The reciprocal of $t_{o1/2}$, represented by $G_{o1/2}$ [Eq. (2)] can also be used as a parameter characterizing the overall crystallization rate of the samples.

$$G_{o1/2} = 1/t_{o1/2} \tag{2}$$

The evolution of crystallinity during isothermal crystallization, the Avrami model[25] is employed to analyze the isothermal crystallization kinetics of the samples. The logarithmic form of Avrami model is expressed as Eq. (3)

$$In[-In(1 - X_t)] = InK_n + nInt \tag{3}$$

where X_t is relative degree of crystallinity at crystallization time t, n is the Avrami exponent, K_n is the crystallization rate parameter involving both the primary nucleation and growth rate of crystals. By fitting the experimental data to Eq. (3) as shown in Figure 2, the values of n and K_n can be obtained from the slope. The $t_{o1/2}$, $G_{o1/2}$, n and K_n are determined and plotted in Figure 3, as a function of isothermal crystallization temperature.

Figures 1–3 show that, the overall crystallization rate parameter $G_{o1/2}$ and the kinetic parameter K_n decrease gradually with the increase of the crystallization temperature, indicating that the overall crystallization rate decreases as the crystallization temperature increases.

Interestingly, the results of PP-A and PP-B are significantly different. As can be seen from Figure 1, the isothermal crystallization temperature of PP-A is obviously higher than that of PP-B, and the time to finish isothermal crystallization for PP-A is obviously shorter than that of PP-B; meanwhile, the results in Figure 3 show that, the $G_{o1/2}$ and K_n of PP-A at higher T_c are obviously higher than that of PP-B at lower T_c. These results above suggest that the overall crystallization rate of PP-A is significantly higher than that of PP-B, it is easier for PP-A to crystallize at relative high crystallization temperature.

Moreover, it can be seen from Figure 3(d) that, as the crystallization temperature increases, the variations of Avrami exponent n of PP-A and PP-B are quite similar. However, the results are obtained at different temperature regions. This result might indicate that the crystallization dimensionalities of PP-A at T_c = 128–132°C are similar with that of PP-B when T_c = 123–127°C.

It is known that, the overall crystallization process comprises two steps, primary nucleation and crystal growth.[26] Both of them will make a contribution to the crystallization process. However, from the study of isothermal crystallization kinetics, the separated contributions of primary nucleation and crystal growth cannot be obtained. Therefore, the self-nucleation isothermal crystallization kinetics and polarized optical microscopy (POM) observation are performed.

Self-Nucleation Isothermal Crystallization Kinetics

In self-nucleation isothermal crystallization kinetics, it is assumed that during the process the sample is fully nucleated. Then the sample was rapidly cooled down and isothermally crystallized at desired temperature. In this way, the subsequent isothermal crystallization can be used to study the crystal growth kinetics.[27]

The curves of the relative degree of crystallinity (X_t) as a function of crystallization time at T_{cSN} of 145, 146, 147, 148, and 149°C are shown in Figure 4. The corresponding exothermic DSC curves at these temperatures are also presented in the inset of Figure 4.

The half crystallization time of crystal growth ($t_{c1/2}$) is direct measure of crystal growth rate. $G_{c1/2}$ (the reciprocal of $t_{c1/2}$) can be used as a parameter to characterize the crystal growth rate. The higher $G_{c1/2}$ is, the faster the crystal growth rate is. The results of $t_{c1/2}$, $G_{c1/2}$ of the samples are plotted in Figure 5 as a function of the crystallization temperature.

On the basis of the Turnbull and Fisher equation, Hoffman and coworkers proposed an equation which is usually referred to as Lauritzen-Hoffman theory [Eq. (4)][28–32]:

$$G = G_0 \exp\left[\frac{-U^*}{R(T_c - T_\infty)}\right] \exp\left[\frac{-K_g}{T_c \Delta T f}\right] \quad (4)$$

where G_0 is the constant and includes all the terms that are temperature-insensitive, G is the crystal growth rate, U^* is the transport activation energy, R is the gas constant and $R = 8.314$, $U^* = 1500$ cal/mol. K_g is the nucleation parameter, T_∞ is the temperature below which motions cease and is usually taken as $T_\infty = T_g$-30K, T_c is the crystallization temperature, $\Delta T = T_m^0 - T_c$ is the degree of undercooling in which $T_m{}^0$ is the equilibrium melting temperature and f is a factor that accounts for the variation in the enthalpy of fusion, Δh_f, with temperature, and is obtained by $f = 2T_c/(T_m^0 + T_c)$.

By rearranging this equation, Eq. (5) is obtained:

$$InG = InG_0 - \left[\frac{U^*}{R(T_c - T_\infty)}\right] - \left[\frac{K_g}{T_c \cdot \Delta T \cdot f}\right] \quad (5)$$

K_g is also expressed as Eq. (6)

$$K_g = n_c b_0 \sigma \sigma_e T_m^0 / \Delta h_f k \quad (6)$$

where the n_c value depends on the crystallization regime according to Lauritzen-Hoffman theory. At Regime I and III which occur at low and high undercoolings, respectively, $n_c = 4$. However, at Regime II, which occurs at medium undercooling, $n_c = 2$. σ and σ_e are the lateral and end surface free energies of the growing crystal, respectively. The b_0 is the molecular thickness, Δh_f is the enthalpy of fusion and k is the Boltzmann constant, $k = 1.38 \times 10^{-23}$ J K^{-1}. It has been reported that, for iPP resins, crystallization occurring with 139–154°C were carried out in Regime II.[33] In this study, since the self-nucleation isothermal crystallization temperature is 142–146°C, n_c is taken to be 2.

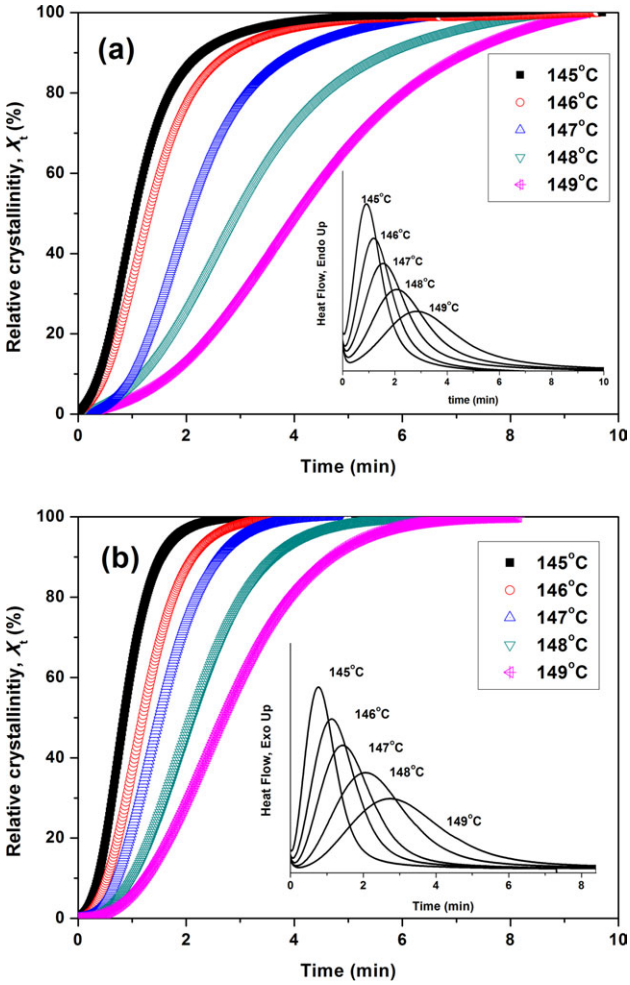

Figure 4. Plots of relative crystallinity versus crystallization time for (a) PP-A and (b) PP-B when isothermally crystallized after self-nucleated at 167 °C. Inset gives the corresponding exothermic DSC curves at these temperatures. [Color figure can be viewed in the online issue, which is available at wileyonlinelibrary.com.]

σ can also be estimated as:

$$\sigma = \alpha \Delta h_f \sqrt{a_0 b_0} \quad (7)$$

where α was empirically obtained to be 0.1 and $a_0 b_0$ represents the cross sectional area of the polymer chain.[34] Δh_f, a_0, and b_0 of iPP are supposed to be 1.96×10^8 J/m^3, 5.49×10^{-10} m and 6.26×10^{-10} m, based on the literature.[35] Therefore, a value of =11.5 erg cm^{-2} is obtained from Eq. (7).

From the plot of $InG + \frac{U^*}{R(T_c - T_\infty)}$ against $\frac{1}{T_c \cdot \Delta T \cdot f}$, the value of K_g can be directly calculated from the slope as shown in Figure 6.

Applied Polymer SCIENCE

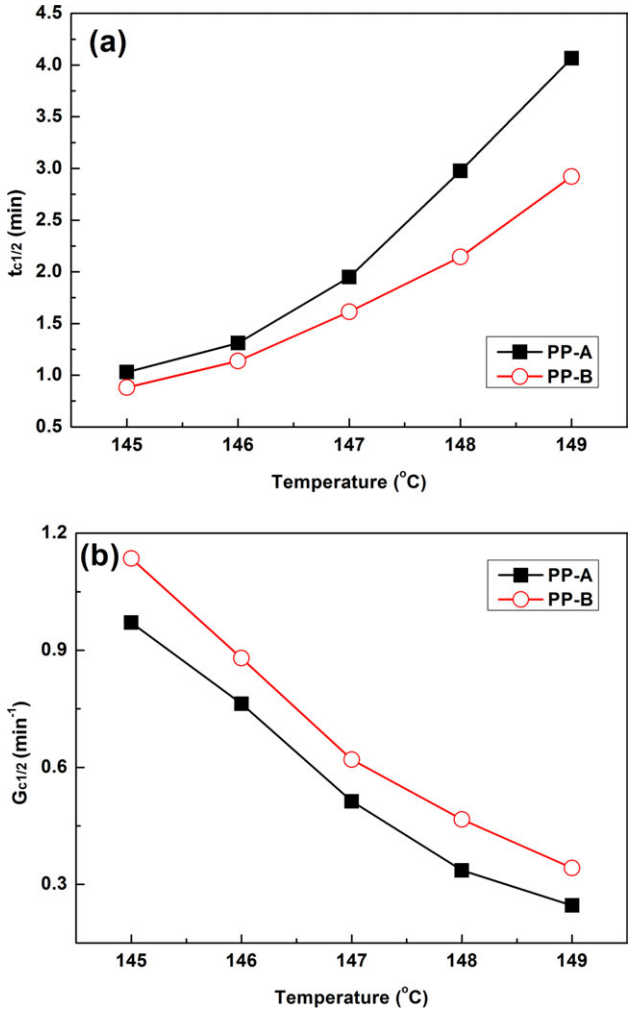

Figure 5. (a) The crystal growth half-time $t_{c1/2}$, and (b) the crystal growth rate parameter $G_{c1/2}$ as a function of crystallization temperature in self-nucleation isothermal crystallization kinetics study. [Color figure can be viewed in the online issue, which is available at wileyonlinelibrary.com.]

Therefore, the value of σ_e was simply estimated by using eqs. (6) and (7) as shown in Table III.

As can be seen from Figure 5 and Table III, at the same crystallization temperature, the $G_{c1/2}$ of PP-B is higher than that of PP-A, and the $t_{c1/2}$ of PP-B is lower than PP-A, indicating the crystal growth rate of PP-B is a little higher than PP-A. On the other hand, the nucleation parameter K_g and the surface free energy σ_e of PP-B are both lower than that of PP-A, suggesting that the energy barrier for the occurrence of crystal growth for PP-B is lower than that for PP-A.

As is studied previously, the overall crystallizability and overall crystallization rate of PP-A is significantly higher than that of PP-B, therefore, the results in Figure 5 and Table II indicate that, the high overall crystallization rate of PP-A is attributed to the high nucleation rate of the sample, namely, the primary nucleation rate of PP-A is believed to be significantly higher than that of PP-B.

From the aspect of molecular structure, the crystallization kinetics of iPP is not only determined by the tacticity (the type, concentration and distribution of the defects), but also influenced by the molecular weight and its distribution. In this study, since the stereo-defect distribution of PP-A and PP-B are quite different from each other, meanwhile the differences in molecular weight and its distribution are close,[21] the main factor that influences the crystallization is the stereo-defect distribution.

Table III. The Secondary Nucleation Parameter $K_g$and the Surface Free Energy of the Growing Crystal σ_e of PP-A and PP-B

Sample	$K_g \times 10^{-4}$ (K^2)	σ_e (erg cm^{-2})
PP-A	27.0	110.3
PP-B	22.1	90.3

Therefore, it can be concluded that in the given polymerization system of this study, a more uniform distribution of stereo-defects of iPP leads to evidently lower nucleation rate; the influence of stereo-defect distribution on the crystal growth kinetics is much less significant than that on primary nucleation. Since PP-A has more amount of PP chains with longer isotactic segments than that of PP-B, it might crystallize at high temperature during the crystallization process and thus act as nuclei to accelerate the overall crystallization rate; on the other hand, PP-B has relative lower amount of high isotactic chains and more amount of chains with medium and low isotactic segments; during crystallization, less amount of nuclei can be formed at high temperature, and the overall crystallization rate of which is lower than PP-A.

Polarized Light Optical Microscopy (POM) Observation

To directly observe the morphology evolution during the crystallization process, the polarized light optical microscopy (POM) observation is performed using a polarized optical microscopy equipped with a hot stage during isothermal crystallization process at 140°C. Figure 7 shows the POM micrographs of PP-A and PP-B.

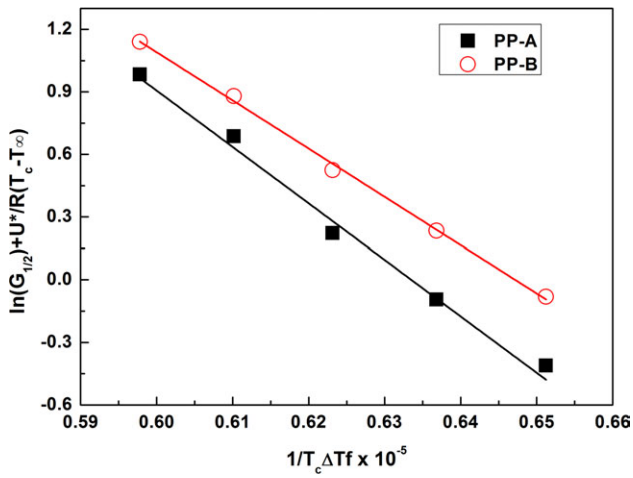

Figure 6. The plots of $\ln(G_{1/2})+(U^*/R(T_c-T_\infty))$ against $1/T_c\Delta Tf$ based on Lauritzen-Hoffman theory for PP-A and PP-B. [Color figure can be viewed in the online issue, which is available at wileyonlinelibrary.com.]

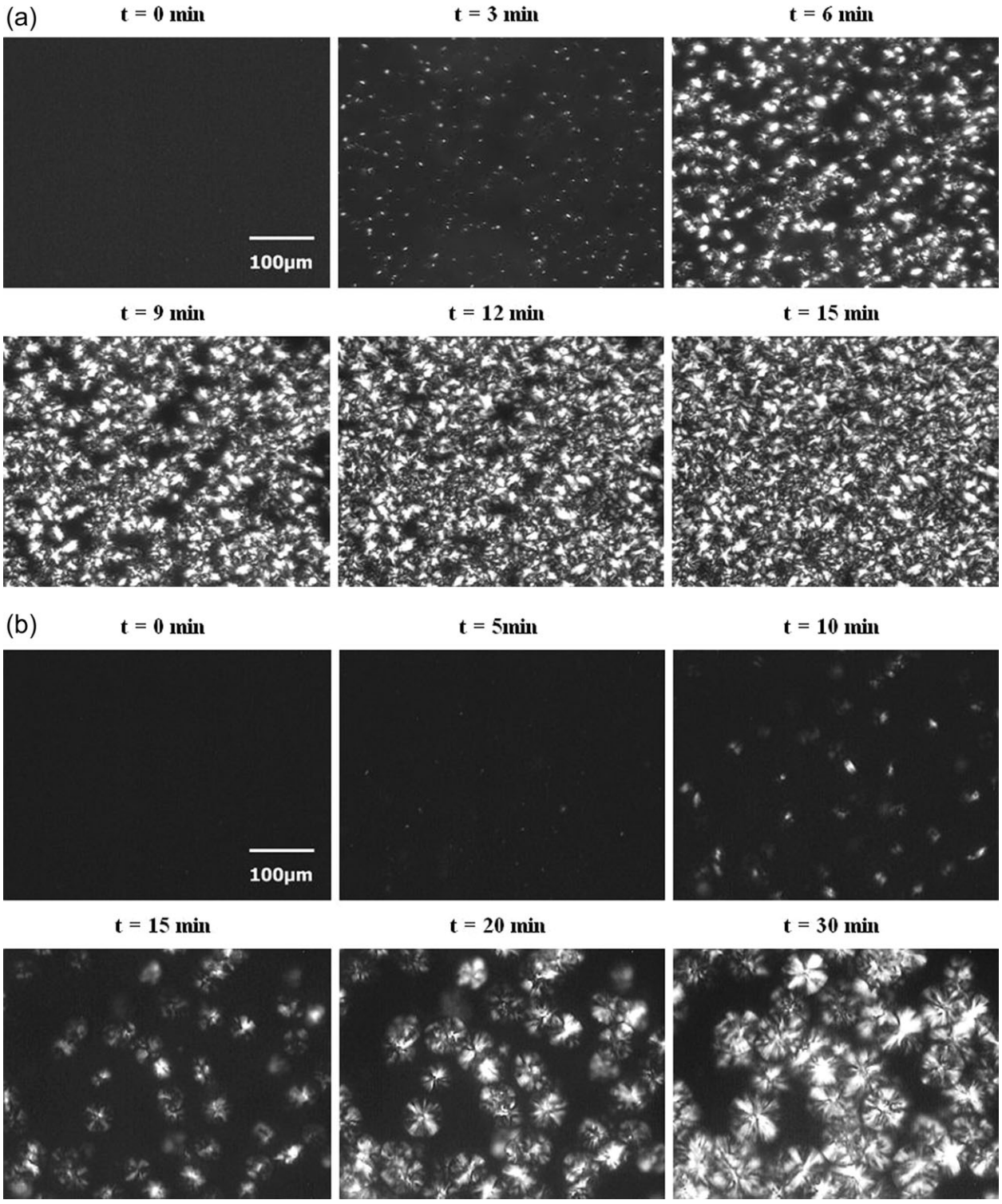

Figure 7. Crystalline morphological evolution of (a) PP-A and (b) PP-B during isothermal crystallization at 140 °C.

Figure 7 shows that the crystallization behavior of PP-A and PP-B are quite different. For PP-A, at 3 min after the crystallization begins, many sporadic nuclei are visible; at 9 min, it is clear that the screen has been nearly full of nuclei, and the small spherulites begin to impinge on each other. At 15 min, the crystallization has gone saturation. For PP-B, surprisingly, at 5 min, only a few small nuclei can be observed; At 10 min, a few more nuclei emerge, but the number of nuclei is much less than that of PP-A; After 15 min of isothermal crystallization, it can be seen that no more nuclei appear, the formed spherulites begin

to grow radially; at 30 min, the spherulites grow continuously, and the crystallization still does not reach saturation.

Compared with PP-B, the nuclei germination of PP-A is much earlier, and the nuclei density of PP-A is much higher. Under the same isothermal crystallization temperature, the number of nuclei formed during a limited crystallization time may represent the nucleation rate of the sample.[36] Therefore, it is obvious that the nucleation rate of PP-A shows a significant promotion compared to PP-B, which is well corresponded with the results of DSC crystallization kinetics studies above.

In general, for Ziegler-Natta iPP, the stereo-defect distribution plays an important role in determining the crystallization kinetics of the resin, including primary nucleation, crystal growth, and overall crystallization. Compared with PP-A, the more uniform stereo-defect distribution of PP-B results in a significantly lower primary nucleation rate, a slightly higher crystal growth rate and a lower overall crystallization. Nucleation rate is more sensitive to stereo-defect distribution than that of crystal growth.

CONCLUSIONS

In this study, the influence of the stereo-defect distribution on the crystallization behavior of ZN-iPP were studied in detail. Two iPP samples with similar average isotacticities but different stereo-defect distribution, polymerized with the same polymerization conditions but different Ziegler-Natta catalysts, were investigated. Attributed to the complexity in ZN-iPP polymerization, it is not easy to adjust the type of catalysts and to obtain ZN-iPP samples with same average isotacticities, but different defect distributions, therefore, the results of this study may bring some new insight on the relationship between stereo-defect distribution and crystallization behavior of ZN-iPP.

The results of isothermal crystallization kinetics, self-nucleation isothermal crystallization kinetics and POM observation show that, for Ziegler-Natta iPP, the stereo-defect distribution plays an important role in determining the crystallization kinetics of the resin, including primary nucleation, crystal growth and overall crystallization. Compared with PP-A, the more uniform stereo-defect distribution of PP-B results in a significant lower primary nucleation rate, a slightly higher crystal growth rate and a lower overall crystallization. Nucleation rate is obviously more sensitive to stereo-defect distribution than that of crystal growth.

ACKNOWLEDGMENTS

The authors express our sincerely thanks to the Program for New Century Excellent Talents in University (NCET-10-0562).

REFERENCES

1. Natta, G.; Pino, P.; Corradini, P.; Danusso, F.; Mantica, E.; Mazzanti, G.; Moraglio, G. *J. Am. Chem. Soc.* **1955**, *77*, 1708.
2. Kang, J.; Yang, F.; Wu, T.; Li, H.; Cao, Y.; Xiang, M. *Eur. Polym. J.* **2012**, *48*, 425.
3. Virkkunen, V.; Laari, P.; Pitkanen, P.; Sundholm, F. *Polymer* **2004**, *45*, 3091.
4. Virkkunen, V.; Laari, P.; Pitkanen, P.; Sundholm, F. *Polymer* **2004**, *45*, 4623.
5. Muller, A. J.; Arnal, M. L. *Prog. Polym. Sci.* **2005**, *30*, 559.
6. Bai, H.; Luo, F.; Zhou, T.; Deng, H.; Wang, K.; Fu, Q. *Polymer* **2011**, *52*, 2351.
7. Luo, F.; Wang, J.; Bai, H.; Wang, K.; Deng, H.; Zhang, Q.; Chen, F.; Fu, Q.; Na, B. *Mater. Sci. Eng. A* **2011**, *528*, 7052.
8. Kang, J.; Chen, J. Y.; Cao, Y.; Li, H. L. *Polymer* **2010**, *51*, 249.
9. Grein, C. *Adv. Polym. Sci.* **2005**, *188*, 43.
10. Lu, H.; Qiao, J.; Yang, Y. *Polym. Int.* **2002**, *51*, 1304.
11. Busico, V.; Cipullo, R. *Prog. Polym. Sci.* **2001**, *26*, 443.
12. Sinn, H.; Kaminsky, W.; Vollmer, H. J.; Woldt, R. *Angew. Chem. Int. Edit.* **1980**, *19*, 390.
13. Kaminsky, W. *Macromol. Chem. Phys.* **1996**, *197*, 3907.
14. Xu, J.; Feng, L. *Eur. Polym. J.* **1999**, *35*, 1289.
15. Yamada, K.; Matsumoto, S.; Tagashira, K. Hikosaka, M. *Polymer* **1998**, *39*, 5327.
16. La Carrubba, V.; Piccarolo, S.; Brucato, V. *J. Appl. Polym. Sci.* **2007**, *104*, 1358.
17. Chen, J.; Yin, L.; Yang, X.; Zhou, E. *Polym. Eng. Sci.* **2004**, *44*, 1749.
18. Lu, H.; Qiao, J.; Xu, Y.; Yang, Y. *J. Appl. Polym. Sci.* **2002**, *85*, 333.
19. Alamo, R. G.; Blanco, J., Agarwal, A. P. K.; Randall, J. C. *Macromolecules* **2003**, *36*, 1559.
20. Alamo, R. G. *Macromol. Symp.* **2004**, *213*, 303.
21. Kang, J.; Yang, F.; Wu, T.; Li, H. L.; Liu, D.; Cao, Y.; Xiang, M. *J. Appl. Polym. Sci.* **2012**, *125*, 3076.
22. Fillon, B.; Wittmann, J.; Lotz, B.; Thierry, A. *J. Polym. Sci. Part B: Polym. Phys.* **1993**, *31*, 1383.
23. Fillon, B.; Thierry, A.; Wittmann, J.; Lotz, B. *J. Polym. Sci. Part B: Polym. Phys.* **1993**, *31*, 1407.
24. Fillon, B.; Lotz, B.; Thierry, A.; Wittmann, J. *J. Polym. Sci. Part B: Polym. Phys.* **1993**, *31*, 1395.
25. Avrami, M. *J. Chem. Phys.* **1940**, *8*, 212.
26. Gedde, U. W. Polymer Physics, Springer, **1995**; p 169.
27. Lorenzo A. T.; Muller, A. J. *J. Polym. Sci. Part B: Polym. Phys.* **2008**, *46*, 1478.
28. Hoffman, J. D.; Miller, R. L. *Macromolecules* **1989**, *22*, 3502.
29. Hoffman, J. D.; Miller, R. L. *Macromolecules* **1988**, *21*, 3038.
30. Hoffman, J. D. *Polymer* **1985**, *26*, 803.
31. Hoffman, J. D. *Polymer* **1985**, *26*, 1763.
32. Lauritzen, J. J. I.; Hoffman, J. D. *J. Appl. Phys.* **1973**, *44*, 4340.
33. Yang, B. X.; Shi, J. H.; Pramoda, K. P.; Goh, S. H. *Compos. Sci. Technol.* **2008**, *68*, 2490.
34. Feng Y.; Hay, J. N. *Polymer* **1998**, *39*, 6723.
35. Clark, E. J.; Hoffman, J. D. *Macromolecules* **1984**, *17*, 878.
36. Xu, W. B. He, P. S. *Polym. Eng. Sci.* **2001**, *41*, 1903.